ORIGINAL RESEARCH PAPER

Encapsulation of Methane Molecules into C_{60} Fullerene Nanocage: DFT and DTFB-MD Simulations

Masoud Darvish Ganji [1], Fahimeh Bonyasi [1], Sepideh Tanreh [1], Mahyar Rezvani [2], Malak Hekmati [1]*

[1] Department of Nanochemistry, Faculty of Pharmaceutical Chemistry, Pharmaceutical Sciences Branch, Islamic Azad University, (IAUPS), Tehran, Iran

[2] Department of chemistry, faculty of science, Arak branch, Islamic Azad University, Arak, Iran

Received: 2017-07-05 Accepted: 2017-08-04 Published: 2017-08-20

ABSTRACT

Extensive urbanization has greatly raised the demand for cleaner coal- and petroleum-derived fuels. Mainly composed of methane, natural gas represents a promising alternative for this purpose, making its storage a significant topic. In the present research, deposition of methane molecules in C_{60} fullerene was investigated through a combined approach wherein density functional based tight binding (DFTB) method was used to optimize the geometry while ab initio density functional theory (DFT) served as a tool for energy calculation. Doping endohedral methane molecules onto fullerene nanocage, it was witnessed that, the only stable complex might be formed by a single methane molecule entrapped inside the C_{60} cage. It was further indicated that, when a large number of encapsulated CH_4 molecules are concerned, occasional chemisorption of the molecules on the inner surface of the cage would occur, ending up breaking the capsule side wall at NCH_4=7. Further studied by density-functional tight-binding molecular dynamics (DFTB-MD) simulation, mechanism of the breakage indicated this complex as being highly unlikely to be stable.

Keywords: *Fullerenes; Methane; Encapsulation; Nanostructures; DFT; Molecular simulation*

How to cite this article

Darvish Ganji M, Bonyasi F, Tanreh S, Rezvani M, Hekmati M. Encapsulation of Methane Molecules into C_{60} Fullerene Nanocage: DFT and DTFB-MD Simulations. J. Nanoanalysis., 2017; 4(2): 159-168. DOI: 10.22034/jna.2017.02.009

INTRODUCTION

Fullerenes are grouped segments of carbon created via closing a graphitic sheet between a fixed quantity of graphitic hexagons and twelve pentagons [1]. Fullerenes comprise a complex class of compounds as they exhibit a myriad of unique attributes. Several various doping possibilities are employed: endohedral (where the fullerene shell encapsulates the dopant), substitutional (dopant included in the fullerene shell), and exohedral (dopant is outside or between shells). Endohedrally doped fullerene has received significant attention as it can be doped by a great number of molecules, including various gases and rare land and transition metal particles (such as K, and La in C_{44}; CCl_2, Co, K, La, and Y in C60) [2]. Detailed analysis of the characteristics of the fullerenes was undertaken subsequent to their discovery in 1991 when different proportions of metals consisting of endohedral fullerenes or metalofullerenes could be manufactured by laser- [3] and arc- [4] vaporization of metal-graphite composites. The initial discovery in 1985 that La atoms might be trapped inside a

* Corresponding Author Email: mhekmatik@yahoo.com

C_{60} cluster to form an endohedral fullerene (La@C_{60} and $La_2@C_{60}$) stemmed from the observation of La-related peaks in the mass spectra of material ejected by laser-vaporization of a La-impregnated graphite target [5, 6]. Additionally, the interaction of C_{60} with a single diatomic molecule encapsulated within the C_{60} (such as $H_2@C_{60}$ [7, 8], $N_2@C_{60}$ [9] and $CO@C_{60}$ [10]) was noticeable; however, according to the reports released until then, there was no interaction between the C_{60} and complexes with two or more molecules.

The Erkoc group's [6, 11] allegation that up to 6 NH3 molecules could be entrapped within a C60 led to the investigation of endohedral complexes of fullerenes with methane molecules.

With ever increasing trend of modern urbanization, demand for clean fuels derived from coal and petroleum has been rapidly increasing. Accordingly, hydrogen and natural gas are usually regarded as suitable non-polluting alternatives to fossil fuel. Therefore, the storage of natural gas, whose main component is methane, has become an important topic. In general, compressed natural gas (CNG) for vehicles is stored in heavy steel cylinders at high pressures (20 to 30 MPa), while adsorbed natural gas (ANG) for vehicles is usually at a relatively more down pressure (i.e. about 4 MPa), so that it can be stored in lightweight containers. Compared to CNG, ANG is a very promising and effective engineering, because the possibility for storage at lower pressure lowers the fuel cost [12,13]. Numerous studies on methane adsorption on porous medium (e.g. molecular sieves, activated carbon, zeolite, etc.) have been reported. Recently, carbon nanotubes have drawn increasing interest because of their unique properties including uniform porosity, high tensile strength, electrical conductivity, and relative inertness. Bekyarova *et al.* investigated the adsorption of methane on a single-walled carbon nanotube (SWCNT) [14], where measured volumetric capacity reached 160 v/v. Kaneko *et al.* also studied the adsorption of methane on SWCNT using a density-functional theory method. They launch that, SWCNT with disordered structure could be used as a storage medium for methane and other supercritical gases [15]. Cao et al. optimized the SWCNT arrays for methane storage at room temperature [16]. In contrast to the many works performed on SWCNT, studies on the adsorption of methane on multi-walled carbon nanotube (MWCNT) are very limited. SWCNTs can be fabricated in various bundle sizes and lengths (i.e. by changing grinding and other mechanical operations) and can contain amorphous carbon. However, MWCNT is capable of making uniform lengths with neither bundle formation nor amorphous carbon content. Therefore, the gas adsorption properties of SWCNT and MWCNT seem to be rather dissimilar.

In a novel study [17], adsorption characteristics of methane (CH_4) were investigated using DFT methods on eight different kinds of hydrogen-capped graphene sheet with different high numbers of carbon atoms. The results were suggestive of higher methane adsorption on defected grouping rather than pristine graphene, and low charge transfer between CH4 and graphene. With its high number of carbon atoms, the physisorbed methane molecule on graphene sheet enhanced adsorption energy to −0.184 to −0.185 eV (pristine graphene) and −0.188 to −0.191 eV (defected graphene). The reduced density gradient (RDG) scatter graph showed the interaction to be weak Van der Waals interaction with the steric repulsion in the graphene sheet.

In our previous work, we studied methane adsorption onto single-wall boron nitride nanotubes (BNNTs) and carbon nanotubes (CNTs) using DFT calculations within the generalized gradient approximation [18]. Structural optimization of several bonding configurations for a CH_4 molecule approaching the outer surface of the (8,0) BNNT and (8,0) CNT showed that, the CH_4 molecule is preferentially adsorbed onto the CNT with a binding energy of −2.84 kcal mol^{-1}. A comparative field of nanotubes with different diameters (curvatures) revealed that, adsorption capacity of methane for on the exterior surface of CNTs is higher for wider CNTs and lower for wider BNNTs. The introduction of defects in the BNNT, significantly enhances methane adsorption. Our first principle findings indicated that, BNNTs might not present a desirable material for natural gas depot.

We also looked into the use of structural defects and nanotube curvature on the adsorption capacity of the SWCNTs [19]. Consequently, larger adsorption energies were observed for metallic CNTs rather than semi-conductive ones. Obtained results for zigzag nanotubes with various diameters revealed that, the adsorption energy is higher for nanotubes with larger diameters. For defected tubes, adsorption energies were estimated for several configurations such as methane molecule approaching the defect sites on pentagons, hexagons, and heptagons on the tube surface. The results displayed that, the introduced defects had an important contribution to the adsorption mechanism of the methane on SWNTs.

We further modeled Si60 fullerene nanocages filled with methane molecules and investigated the capability of such endohedral fullerene for energy storage [20].

Ab initio calculations at the Density Functional level of Theory (DFT) showed that upwards to eight CH4 molecules being incorporated inside the cage can form the stable complex with Si60 fullerene. Our calculated results revealed a substantial growth in the storage capacity of methane inside Si60 fullerenes compared with C60 fullerenes.

We further modeled Si60 fullerene nanocages filled with methane molecules and investigated the capability of such endohedral fullerene for energy storage [20]. *ab initio* calculations using DFT showed that, up to eight CH_4 molecules being incorporated inside the cage can form a stable complex with Si60 fullerene. Our calculated results revealed a significant increase in the storage capacity of methane inside Si60 fullerenes compared to that of C_{60} fullerenes.

The objective of the present research is to enhance our understanding of the stability of endohedral methane-doped fullerene ($n CH_4@C_{60}$) through the application of DFT-based computations. Moreover, the dispersion correction for the vdW interaction has been acknowledged in this work. Considering the issues associated with locating materials for gas storage, relative simplicity of undertaking calculations in software packages based upon standard DFT, the use of this method is greatly desirable and deserves deliberation.

COMPUTATIONAL METHODS

The newly designed DFTB+ code optimizes C_{60} and methane molecules [21] using a Density-Functional Tight-Binding (DFTB) procedure based on a second-order expansion of the Kohn-Sham total energy in DFT with respect to the charge density fluctuations. Employing the second-order expansion, a transparent, parameter-free, and readily calculable expression for generalized Hamiltonian matrix elements can be derived. These are modified by a self-consistent redistribution of Mulliken charges (SCC). In one hand, unlike the typical Hartree-Fock approximation methods or conventional DFT, DFTB uses a tabulated set of integrals derived from *ab initio* DFT calculations [22], leading to a substantial speed-up of the method. On the other hand, unlike conventional tight-binding, DFT-based DFTB can be used to undertake parameterizations at an accuracy close to that of LDA/GGA with minimal adjustable parameters, and is transferable between different systems. In DFTB, basis functions are also available, allowing the reconstruction of actual wave functions from the calculations. The electronic part contains atomic and diatomic contributions which are both calculated from an atomic DFT program using either LDA or GGA function. The repulsive energy contribution is approximated as a sum of pair potentials, which are represented either by spline functions or by polynomials. Further details of the method have been fully reviewed for instance in [21-23]. In this work, the Slater-Koster (S-K) type parameter set [24] was implemented. Furthermore, the dispersion was corrected for Van der Waals interaction via Slater-Kirkwood type model [25].

The DF-TBMD simulations are done by DFTB+ in the canonical regime; i.e., the thermodynamical system under consideration is described by the number of particles N, volume V, and temperature T as variables. The structure under study is in contact with Andersen thermostat [26] having fixed temperature 300 K. The MD time step is 1.0 fs.

The accuracy of our method is tested by comparison of optimized geometries of fullerene C_{60} against the existing experimental data. The calculated and experimental [27] bond lengths of the single C–C bond of C_{60} molecule (i.e., the C5–C6) are 1.455 and 1.458 Å, while for the double bond of the fullerene (i.e., the C6–C6) these values are 1.404 and 1.401 Å, respectively. From the consistency of these results, we conclude that the DFTB is suitable and effective for geometry optimization of fullerenes.

All DFT calculations were performed utilizing ORCA version 3.0.3 (a quantum chemistry program) which is based on a localized basis set and all-electron DFT calculations [28]. The single-point energy (SPE) calculations were carried out using the B3LYP [29, 30] functional as the exchange–correlation part which exhibited the best performance and accuracy in Grimme's GMTKN30 benchmark set [31] together with the Ahlrichs split-valence def2-TZVP basis set [32]. The coulomb part was integrated using the Resolution of Identity (RI) approximation, with the decontracted form of the def2-TZVP/J basis set been selected for this purpose [33–37]. The Lebedev434 grid (Grid5) was set for DFT integration in the SCF cycle and also final energy calculations.

The third version of empirical dispersion corrections, as proposed by Grimme in combination with the Becke–Johnson damping (D3BJ) method, together with the contribution of three-body dispersion terms was employed to account for the long-range dispersion interactions in both geometry optimizations and energy calculations [38, 39]. The crucial role of dispersion interactions in carbon

nanostructures has been highlighted in several theoretical studies including a study by Martinez *et al*. where inclusion of the dispersion terms led to obtaining values similar to the experimental results [40]. In order to evaluate stability of the endohedral fullerene, values of binding energy, E_b, of the interacting systems were calculated. The binding energy values were achieved by using the following equation:

$$E_b = E\,(C_{60}/CH_4) - [E(C_{60}) + E(CH_4)] - EBSSE \qquad (1)$$

where $E(C_{60}/CH_4)$ is total energy of the fullerene interacting with methane molecule, $E(C_{60})$ is total energy of the free C_{60} fullerene, $E(CH_4)$ is total energy of a methane molecule, and EBSSE refers to the basis set superposition error computed via counterpoise method which is employed to reduce the effect of basis set incompleteness.

RESULT AND DISCUSSION

Trying to investigate stability of the $n CH_4@C_{60}$ systems, we began with examining the binding energies (formation energy) of CH_4 molecules inserted into C_{60} cage. The binding energy is calculated as follows:

$$E_b = E_{C60\text{-}nCH4} - E_{C60} - nE_{CH4} \qquad (2)$$

where $E_{C60\text{-}nCH4}$ is total energy of the C_{60} with n encapsulated methane molecules in C_{60} skeleton, E_{C60} is total energy of pure C_{60}, and E_{CH4} is total energy of isolated methane molecule.

Optimized C_{60} cage structure was used for the molecular interactions. Accordingly, firstly, $1CH_4@C_{60}$ complex was optimized with DFT-B3LYP model. After full structural optimization of the complex, it was found that the value of binding energy is negative for one encapsulated CH_4 molecule. The calculated binding energy was determined to be -0.47 eV. Further evaluated was the effect of BSSE on the binding energy estimation, and the calculated E_b (-0.46 eV) was found to be rather the same as the result of conventional estimation. In the next step, the $1CH_4@C_{60}$ complex was optimized with DFTB method and the binding energy was calculated at DFT-B3LYP level. Following this procedure, the binding energy was estimated to be -0.48 eV, i.e. the same as that of the optimized system with DFT-B3LYP model. For the $1CH_4@C_{60}$ complex, average bond length of C–H in the methane changed to 1.078 Å, which is basically the same as that for an isolated CH_4 molecule (1.089 Å). The calculated average C....H distance (C atom of the C_{60} cage and H atom of the methane) at equilibrium was about 2.490 Å (see Fig. 1a). The calculated binding energy and equilibrium distances were comparable with those of amino acids, nucleic acid bases, and gas molecules interacting with carbon-based nanostructures [41-49]. The small binding energy and change of the C–H bond indicated physisorption between the methane molecule and the C_{60} cage.

In order to investigate methane storage capability of fullerene C_{60}, interaction of CH_4 molecules attached to outer sidewall of the nanocage was further evaluated. To this end, a CH_4 molecule was placed onto both hexagonal and pentagonal rings of the nanocage followed by optimizing the modeled system. After full structural optimization of the whole system, it was found that, the methane molecule prefers to be adsorbed on the cage over its hexagonal ring, as depicted in Fig. 1b. The obtained binding energy and adsorption distance between the interacting molecules were determined to be -0.07 eV and 3.00 Å, respectively. As can be seen from the binding parameters, the methane adsorption on the nanocage was found to be of weak physisorption nature [47-49].

To give further insight into the nature of the interaction between methane molecule and C_{60} fullerene, charge population and charge density analyses were performed for the complexes under consideration. The charge analysis indicated that, a small charge has been transferred from the adsorbed methane molecule to the nanocage (0.001 *e*), while significant charges were transferred from the nanocage to incorporated methane molecule (0.34 *e*). These findings confirmed the calculated binding energies for the considered adsorption configurations. The calculated electron density also revealed that, there was physical interaction between both attached and incorporated methane molecules to the C_{60} fullerene nanocage. Figs. 1 (c) and (d) demonstrate that, there is no charge density at interface media of the systems under study. Furthermore, the calculated highest occupied molecular orbitals (HOMO) and lowest unoccupied molecular orbitals (LUMO) showed that the majority of both HOMO and LUMO are localized on the nanocage (as shown in Fig. 1(e)). This indicates that, C_{60} cage skeleton is an electron source which serves as an electron donor for encapsulated methane molecule.

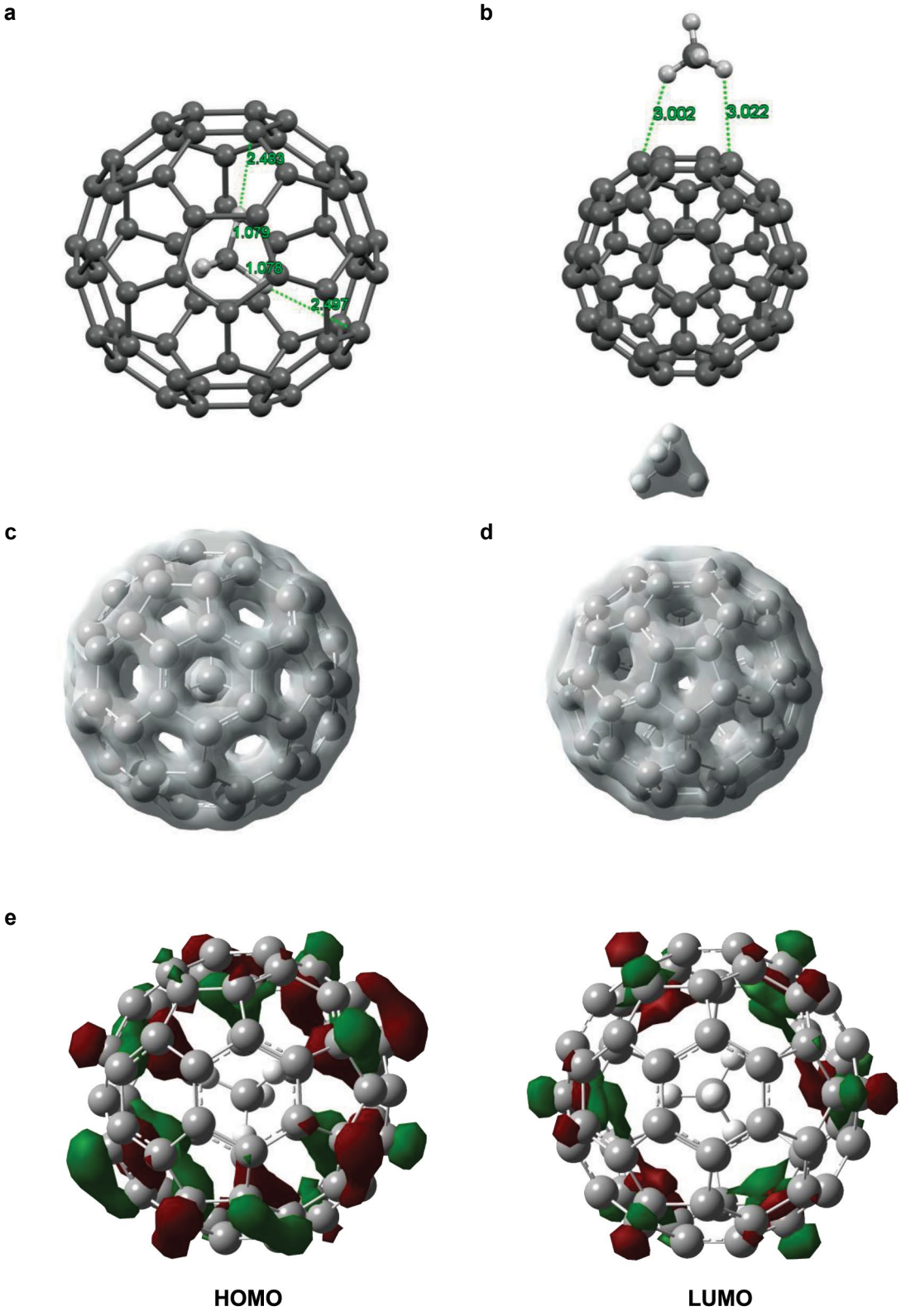

Fig. 1. Optimized geometries of (a) $1CH_4@C_{60}$ and (b) adsorbed CH_4 molecule onto C_{60} nanocage (CH_4/C_{60}). Carbon and hydrogen atoms are shown in gray and white colors, respectively. Calculated charge density of (c) $1CH_4@C_{60}$ and (d) CH_4/C_{60} complexes. (e) HOMO and LUMO states of $1CH_4@C_{60}$ complex.

In the next step, encapsulation of further methane molecules inside the C_{60} nanocage was evaluated. DFTB method was used for structural optimization of the considered complexes and then binding energies were determined at DFT-B3LYP level. All the structures with larger *n* had positive formation energies, making them metastable. Table 1 shows binding energies of $nCH_4@C_{60}$ type (*n*: 1–3) systems. The ability of C_{60} fullerene to encapsulate methane by incorporating more molecules into the cage was further studied. Fig. 2 shows some typical optimized geometries of $nCH_4@C_{60}$ for *n*=2–4 and 7. The figure shows that, the fullerene shape deviates from a sphere at higher number of encapsulated methane molecules, as is clear from Fig. 2(d). For a relatively small number of encapsulated methane molecules, i.e. *n* <4, all the methane inside C_{60} existed only in molecular form. As it can be seen from the figure, when 4 CH_4 molecules were encapsulated into the C_{60} cage, a new bond between an H atom and C_{60} was formed. Furthermore, the length of the C=C bond, which was saturated with the H of CH_4, changed from 1.445 to 1.504 Å, indicating that the C=C double bond was transformed into a C–C single bond. However, for 7 $CH_4@C_{60}$ system, surprisingly, the C_{60} cage was seen to break, so that some methane molecules escape from the cage. Accordingly, this system seems to be highly improbable.

Table 1. Calculated binding energies (formation energy) E_B (eV) for $nCH_4@C_{60}$ type (*n*: 1–3) complexes

$nCH_4@C_{60}$	$1CH_4$	$2CH_4$	$3CH_4$
E_B (eV)	-0.48	3.35	1108.14

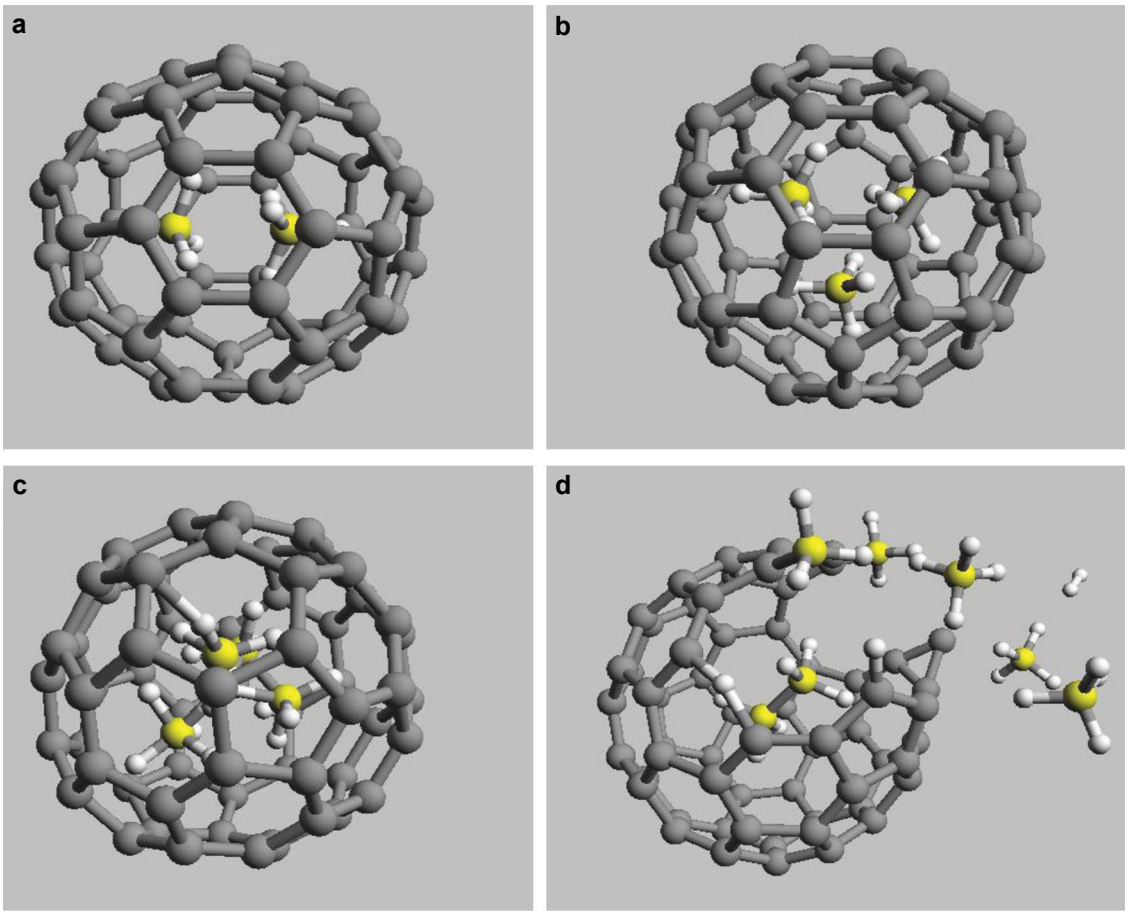

Fig 2. Optimized geometries of $nCH_4@C_{60}$ structures with (a) n=2, (b) n =3, (c) n=4, and (d) *n* CH_4=7. Carbon and hydrogen atoms are shown in gray (yellow for the methane) and white colors, respectively.

Following with the research, the relationship between the number of encapsulated CH_4 molecules and the associated repulsive energies in the confined system was investigated (total energies were calculated with DFTB method). In Fig. 3, the variation of the energy per CH_4 molecule to the number of the confined CH_4 molecules is carefully examined. The corresponding average CH_4–CH_4 and CH_4–C_{60} repulsive energies were calculated by the following equations [50-52]:

$$E_{rep}(CH_4\text{-}CH_4)=(E_{total\,(nCH4)} - E_{total\,(nCH4)} - E_{CH4})/NCH4 \quad (3)$$

and

$$E_{rep}(CH_4\text{-}C_{60})=(E_{total\,(CH4\text{-}C60)} - E_{total\,(nCH4)} - E_{C60})/NCH_4 \quad (4)$$

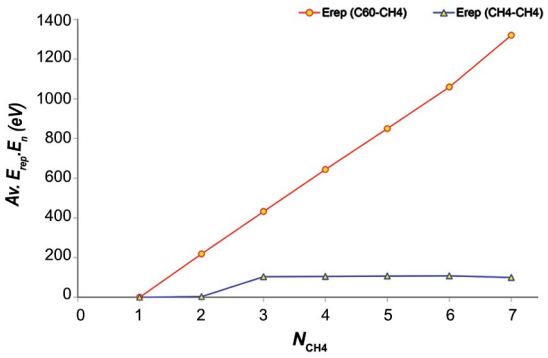

Fig. 3. Variation of average CH_4–CH_4 and C_{60}–CH_4 repulsive energies with the number of CH_4 molecules confined in C_{60} fullerene.

where $E_{total}(nCH_4)$ is total energy of all the CH_4 molecules in the C_{60}, E_{CH4} is the energy of a single CH_4 molecule confined in the fullerene, N_{CH4} is total number of methane molecules in the system, and $E_{total}(CH_4–C_{60})$ and E_{C60} are total energies of the system with and without encapsulated methane molecules, respectively.

Fig. 2 demonstrates that both repulsive energies are positive, and that the distance separating the methane molecules and the fullerene wall is typically greater than the distance between the methane molecules. When only one CH_4 molecule is encapsulated into the C_{60}, the presented results show that the molecule behaves as a free molecule and resides at the center of the cage, because the distance between the center of the cage and the carbon cage shell is about 3.7 Å, which is too large for any bonding interaction between methane and carbon. But with more methane molecules being encapsulated, the formation of various methane molecular clusters within the C_{60} develops a variety of well-defined shapes, and the CH_4–CH_4 repulsive energy begins to increase.

With increasing the quantity of CH_4 molecules, the rate of increase in the CH_4-C_{60} repulsive energy becomes gradually greater than the rate of increase in the CH_4-CH_4 repulsive energy. On the other hand, it is observed that, with the initial increase in the number of encapsulated CH_4 molecules, average CH_4–C_{60} repulsive energy increases until N_{CH4}=6, but with subsequent increase in N_{CH4}, it rises quickly until N_{CH4}=7. It can also be seen from the figure that, with the initial increase in the number of encapsulated CH_4 molecules, average CH_4–CH_4 repulsive energy remains constant until N_{CH4}=2. However, when N >3 molecules were encapsulated into the C_{60} cage, the CH_4–CH_4 repulsive energy increased slowly with the initial increase in the number of encapsulated CH_4 molecules, thereby forming a new bond between CH_4 molecule(s) and C_{60} which increased the CH_4–C_{60} repulsive energy slowly. For the case where 7 CH_4 molecules were encapsulated into the C_{60} cage, the CH_4–C_{60} repulsive energy was seen to increase to the extent where wall of the cage broke eventually and some of the CH_4 escaped from the cage. In this case, it was evident that the repulsive interactions between the encapsulated CH_4 molecules and the fullerene wall as well as that between the methane molecules themselves play an important role in determining the structural states of the CH_4@C_{60} complexes.

In order to study the opening of the wall of the C_{60} by increasing CH_4 molecules, a DF-TBMD simulation for 7 CH_4 molecules being trapped within the C_{60} cage was completed. The mechanism of cage opening is illustrated in Fig. 4. Accordingly, 7 CH_4@C_{60} complexes were placed in contact with a thermostat at room temperature. Being very long (up to 1.704 Å), the C–C bonds of the fullerene cage are very weak and easy to break. Due to the large number of methane molecules encapsulated in the fullerene cage, a large number of carbon atoms of the C_{60} are hydrogenized. As it can be seen from the figure, at 10 fs, an H atom bridges two adjacent C atoms via covalent bonds. Behavior of these two carbon atoms is especially important for the process of fullerene breakage. One of them (denoted as $C_{H\text{-}1}$) is situated closer to the nearest hydrogen atom, as compared to the other C atom (denoted as $C_{H\text{-}2}$) ($C_{H\text{-}1}$–H and $C_{H\text{-}2}$–H distances are 1.236 and 1.388 Å, respectively).

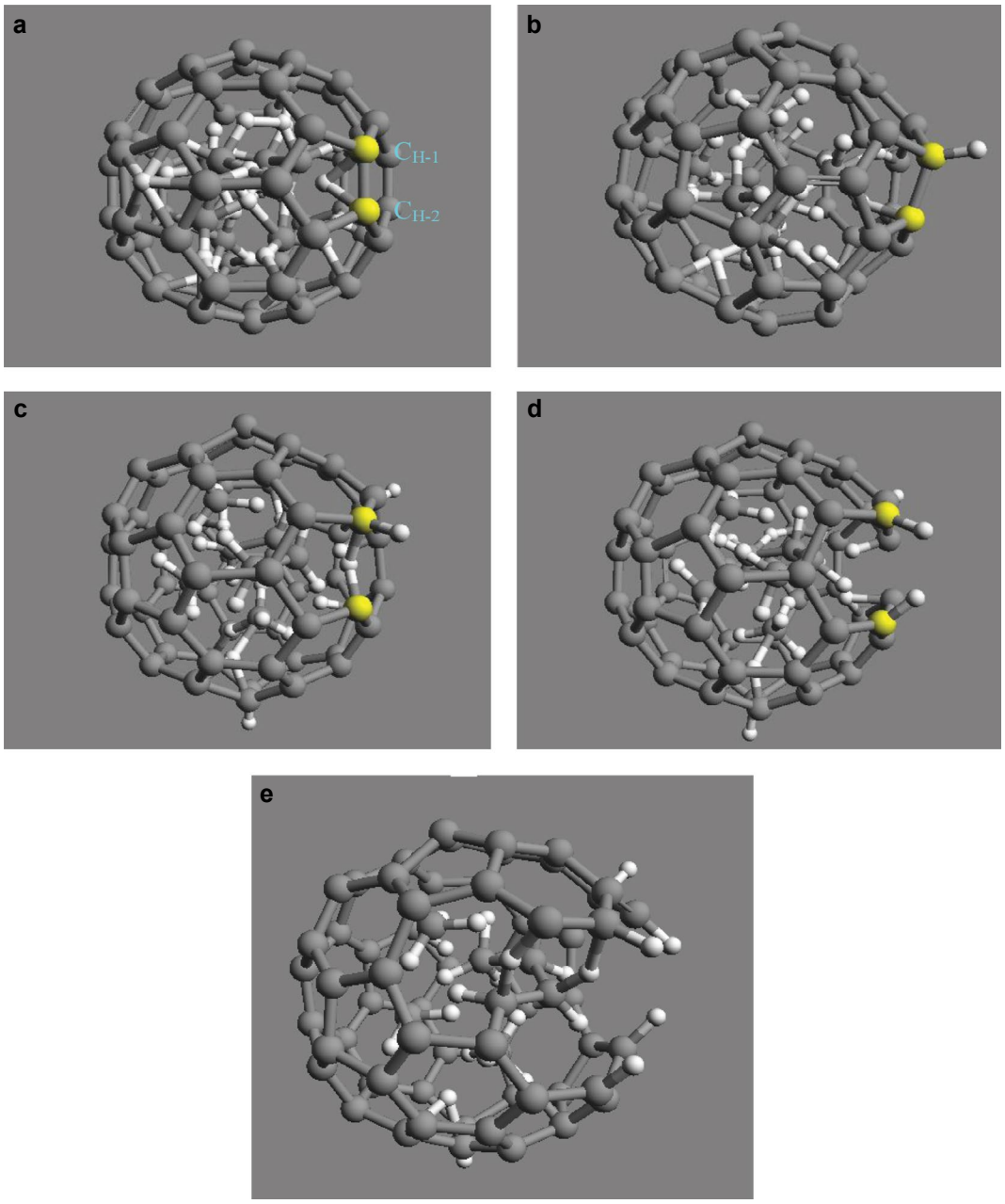

Fig. 4. Snapshots of DFT-based tight binding molecular dynamics simulations of $7CH_4@C_{60}$ structure at 300 K: (a) 10 fs, (b) 70 fs, (c) 765 fs, (d) 885 fs and (e) 1250 fs.

Atomic movements during MD simulations led to the hydrogenation of C_{H-1} atom. Accordingly, the partial π-bond between C_{H-2} and H atom broke, followed by the breakage of C_{H-2} bonds with the other H atom. As one can see from Fig. 4 (c), the length of the C_{H-2}–C_{H-1} bond extended to 2.203 Å, causing the bond to break after 765 fs (Fig. 4 (c)). Then, the hydrogen bound to C_{H-1} quickly changed its position, such that this carbon atom restored sp hybridization. Internal pressure pushed hydrogen atom toward the opened hole on the fullerene surface. Further atomic movements during MD simulations led to increased hydrogenation of C atoms (after 1250 fs), leading to a CH_2-group formation, as shown in Fig. 4(e). This made the process of fullerene breakage irreversible. It could be concluded that the cage opening is promoted by the breakage of one of the weak C-C bonds

formed by two carbon atoms, all of whose nearest neighbors are fully or partially hydrogenized. Thus, C_{60} nanocage was found not to be capable of accommodating 7 methane molecules.

CONCLUSION

Endohedral methane-doped C_{60} systems, $n$$CH_4$@$C_{60}$ (n: 1–7), were theoretically tested at the level of density functional theory type treatment. The CH_4-CH_4 and CH_4-wall repulsive energies as well as the $n$$CH_4$@$C_{60}$ formation energy were computed as functions of the number of trapped methane molecules, N_{CH4}.

According to the results, it was evident that the C_{60} cage could hold a great number of methane molecules, and despite their significantly endothermic nature, such structures (with a large amount of trapped methane) are metastable. For larger n values, it was determined that a fraction of the hydrogen atoms of methane could be chemisorbed on the interior of the cage (by forming covalent C-H bonds). Up to 6 methane molecules (N_{CH4}=6) could be stored within the C_{60} to form a metastable structure. Such a structure could also be achieved with higher number of methane molecules, but only under increased pressure.

It was demonstrated that, for 7 methane molecules (N_{CH4}=7) the cage wall eventually collapsed and the collapse mechanism was analyzed via density functional theory-based tight binding molecular dynamics (DF-TBMD) simulations, thus this complex seems to be significantly unlikely. It has also been demonstrated that, the weakening of the fullerene C-C bonds during the hydrogen chemisorption is the major reason behind the opening of the nanocage. To further enhance the knowledge of these $(CH_4)_n$@C_{60} systems, further research still needs to be undertaken.

ACKNOWLEDGMENT

The authors acknowledge and are grateful for the support of this undertaking by the Faculty of Pharmaceutical Chemistry, Pharmaceutical Sciences Branch, Islamic Azad University (IAUPS), Tehran, Iran.

CONFLICT OF INTEREST

The authors declare that there is no conflict of interests regarding the publication of this manuscript.

REFERENCES

1. H. W. Kroto, Int. J. Mass Spectrometry & Ion Processes (1994) 138, 1.
2. M. S. Dresselhaus, G. Dresselhaus, P. C. Eklund, Science of Fullerens and Carbon Nanotubes, (Academic Press-San Diego 1996).
3. Y. Chai, T. Guo, C. M. Jin, R. E. Haufler, L. P. F. Chibante, J. Fure, L. H. Wang, J. M. Alford, R. E. Smalley, J. Phys. Chem. (1991) 95, 7564-7568.
4. R. D. Johnson, D. S. Bethune, C. S. Yannoni, Acc. Chem. Res. (1992) 25, 169-175.
5. J. R. Heath, S. C. O'Brien, Q. Zhang, Y. Liu, R. F. Curl, H. W. Kroto, F. K. Tittel, R. E. Smalley, J. Am. Chem. Soc. (1985) 107, 7779-7780.
6. S. Erkoc¸ L. Turker, J. Mol. Struct. (Theochem) (2003) 640, 57-63.
7. Y. Murata, M. Murata, and K. Komatsu, J. Am. Chem. Soc. (2003) 25, 7152-7153.
8. K. Komatsu, M. Murata, and Y. Murata. Science (2005) 307, 238-240.
9. T. Suetsuna, N. Dragoe, W. Harneit, A. Weidinger, H. Shimotani, S. Ito, H. Takagi, and K. Kitazawa. Chem. Eur. J. (2002) 70, 5079-5083.
10. T. Peres, B. P. Cao, W. D. Cui, A. Khong, R. J. Cross, M. Saunders and C. Lifshitz .Int. J. Mass Spectr.(2001) 210, 241-250.
11. L. Turker, S. Erkoc. J. Mol. Struct. (Theochem) (2003)638, 37-42.
12. D. Lozano-Castello, J. Alcaniz-Monge, M. A. de la Casa-Lillo, D. Cazorla-Amoros. Fuel (2002) 81, 1777-1803.
13. B. U. Choi, D. K. Choi, Y. W. Lee, B. K. Lee, S. H. Kim. J. Chem. Eng. Data (2003) 48, 603- 607.
14. E. Bekyarova, K. Murata, M. Yudasaka, D. Kasuya, S. Iijima, H. Tanaka, H. Kahoh, K. Kaneko, J. Phys. Chem. B (2003) 107, 4681-4684.
15. H. Tanaka, El. El-Merraoui, W. A. Steele, , K. Kaneko. Chem. Phys. Lett. (2002) 352, 334-341.
16. D. Cao, X. Zhang, J. Chen , W. Wang, J. Yun. J. Phys. Chem. B (2003) 107, 13286-13292.
17. V. S. Anitha, R. Shankar, S. Vijayakumar, Stru.Chem(2017), 1-18.
18. M.D. Ganji, A. Mirnejad and A. Najafi, Sci. Technol. Adv. Mater. (2010) 11, 045001.
19. M.D. Ganji, M. Asghary, and A.A. Najafi, Commun. Theor. Phys. (2010) 53, 987–993.
20. M. D. Ganji, M. Rezvani, M. Shokry And A. Mirnejad, Fullerenes, Nanotubes, and Carbon Nanostructures,(2011) 19, 421–428.
21. B. Aradi, B. Hourahine and Th. Frauenheim, J. Phys. Chem. A. (2007) 111, 5678.
22. G. Seifert, D. Porezag and Th. Frauenheim, Int. J. Quantum Chemistry. (1996)58, 185.
23. Th. Frauenheim, G. Seifert, M. Elstner, Z. Hajnal, G. Jungnickel, D. Porezag, S. Suhai, and R. Scholz, Phys. Stat. Sol.(2000) 271, 41.
24. M. Elstner, D. Porezag, G. Jungnickel, J. Elsner, M. Haugk, Th. Frauenheim, S. Suhai, and G. Seifert.Phys. Rev. B.(1998) 58, 7260.
25. M. Elstner, P. Hobza, Th. Frauenheim, S. Suhai, and E. Kaxiras , J. Chem. Phys (2001) 114, 5149.
26. H. C. Andersen, J. Chem. Phys.(1980) 72, 2384.

27. K. Hedberg, L. Hedberg, D. S. Bethune, C. A. Brown, H. C. Dorn, R. D. Johnson, M. De Vries,Science (1991) 254 410.
28. F. Neese, Wiley Interdiscip. Rev. Comput. Mol. Sci, (2012) 2, 73–78.
29. A.D. Becke, J. Chem. Phys.(1993) 98, 5648-5652.
30. C. Lee, W. Yang, R.G. Parr, Phys. Rev. B (1988) 37, 785-789.
31. L. Goerigk and S. Grimme, Phys. Chem. Chem. Phys,(2011) 13, 6670–6688.
32. F. Weigend and R. Ahlrichs, Phys. Chem. Chem. Phys, (2005)7, 3297–3305.
33. E. Baerends, D. Ellis and P. Ros, Chem. Phys, (1973) 2, 41–51.
34. B. I. Dunlap, J. Connolly and J. Sabin, J. Chem. Phys, (1979) 71, 3396–3402.
35. C. Van Alsenoy, J. Comput. Chem, (1988) 9, 620–626.
36. R. A. Kendall and H. A. Fru¨chtl, Theor. Chim. Acta (1997) 97, 158–163.
37. K. Eichkorn, F. Weigend, O. Treutler and R. Ahlrichs, Theor. Chim. Acta (1997) 97, 119–124.
38. S. Grimme, J. Antony, S. Ehrlich and H. Krieg, J. Chem. Phys, (2010) 132, 154104.
39. A. D. Becke and E. R. Johnson, J. Chem. Phys, (2005) 123, 154101.
40. S. H. Martı´nez, S. Pan, J. L. Cabellos, E. Dzib, M. A. Ferna´ndez-Herrera and G. Merino, Organometallics (2017) 36, 2036–2041.
41. J. Zhao, A. Buldum, J. Han, and J.P. Lu, Nanotechnology, (2002) 13, 195.
42. I. Cabria, M. J. Lopez, J. A. Alonso, Eur. Phys. J. D. (2005) 34, 279.
43. M. D. Ganji, Nanotechnology, (2008) 19, 025709.
44. M. D. Ganji, Phys. Lett. A , (2008) 372, 3277.
45. M. D. Ganji, Phys. E (2009) 41, 1406.
46. M. D. Ganji, Diamond Related Mater (2009) 18, 662.
47. M. D. Ganji , Phys. E (2009)41, 1433.
48. M. D. Ganji, S. M. Hosseini-khah and Z. Amini-tabar, Phys. Chem. Chem. Phys, (2015) 17, 2504-2511.
49. M. D. Ganji, N. Ahmadian , J. Nanoanalysis, (2016) 3, 58-68.
50. R. E. Barajas-Barraza, R. A. Guirado-Lopez, Phys. ReV. B (2002) 66, 155426.
51. T. A. Murphy, T. Pawlik, A. Weidinger, M. Hőhne, R. Alcala, J. M. Spaeth, Phys. Rev. Lett. (1996)77, 1075.
52. Y. X. Ren, T. Y. Ng, K. M. Liew, Carbon (2006) 44, 397.